



Cite this: *Chem. Commun.*, 2015, 51, 9227

Received 28th February 2015,  
Accepted 28th April 2015

DOI: 10.1039/c5cc01758k

www.rsc.org/chemcomm

## Structural snapshots of the SCR reaction mechanism on Cu-SSZ-13†

Tobias Günter,<sup>a</sup> Hudson W. P. Carvalho,<sup>a</sup> Dmitry E. Doronkin,<sup>ab</sup> Thomas Sheppard,<sup>a</sup> Pieter Glatzel,<sup>c</sup> Andrew J. Atkins,<sup>d</sup> Julian Rudolph,<sup>e</sup> Christoph R. Jacob,<sup>de</sup> Maria Casapu<sup>a</sup> and Jan-Dierk Grunwaldt<sup>\*ab</sup>

**The structure of copper sites in Cu-SSZ-13 during NH<sub>3</sub>-SCR was unravelled by a combination of novel operando X-ray spectroscopic techniques. Strong adsorption of NH<sub>3</sub> on Cu, its reaction with weakly adsorbed NO from the gas phase, and slow re-oxidation of Cu(I) were proven. Thereby the SCR reaction mechanism is significantly different to that observed for Fe-ZSM-5.**

Selective catalytic reduction of NO<sub>x</sub> by ammonia (NH<sub>3</sub>-SCR) over iron and copper based catalysts is presently the predominant way to remove hazardous NO<sub>x</sub> from automotive exhaust gases.<sup>1</sup> In particular the chabazite-based catalysts Cu-SSZ-13 and Cu-SAPO-34 have recently attracted strong interest due to their outstanding performance and hydrothermal stability.<sup>2</sup> Although Cu-SSZ-13 has already been commercialized, the reaction mechanism and the structure of the active sites are still strongly debated.<sup>3</sup> Typically, single Cu<sup>2+</sup> sites are located close to a six- or eight-member ring (6MR or 8MR).<sup>4</sup> They are mobile, dynamically change their structure,<sup>4c</sup> and less active Cu dimers can be formed at intermediate temperatures.<sup>5</sup> This structural variation inevitably requires operando studies.

*In situ* X-ray absorption spectroscopy (XAS) has uncovered high redox dynamics of Cu sites in the chabazite framework, particularly promoted during the standard SCR process.<sup>4b,6</sup> This redox behavior, which is similar to Fe-zeolites, originates from the reaction of NO and NH<sub>3</sub>.<sup>7</sup> The reduction of Cu<sup>2+</sup> sites was observed also in an NH<sub>3</sub> containing stream.<sup>7,8</sup> Nevertheless, the nature of adsorbed species and the sequence of reaction steps are still controversial. For large-pore zeolites the reaction between gaseous or oxidatively adsorbed

NO and adsorbed NH<sub>3</sub> has been proposed.<sup>6a,9</sup> Oxidative adsorption of NO<sub>x</sub> together with stronger non-dissociative adsorption of NH<sub>3</sub> on Cu sites has been reported on both Cu-SAPO-34 and Cu-SSZ-13.<sup>10</sup> Furthermore, formation of nitrosyl groups NO<sup>+</sup> has been found by IR spectroscopy.<sup>11</sup> The interaction of Cu<sup>2+</sup> sites in Cu-SAPO-34 with both NO and NH<sub>3</sub> was further evidenced by *in situ* EPR.<sup>12</sup> With respect to the influence of other gaseous species, a positive effect of water for the SCR reaction has been reported, although it strongly inhibits NO oxidation.<sup>3,13</sup> However, most of the studies that can evidence the interaction between the adsorbates and copper were not performed under operating conditions, which appears particularly important as previously demonstrated by Ribeiro *et al.*<sup>4b,14a</sup> Recent investigations have shown that combined synchrotron-based hard-X-ray photon-in/photon-out techniques<sup>15</sup> allow probing *in situ* not only the oxidation state and the coordination sphere but also the nature of the ligands.<sup>8,14b</sup>

Here we report on the use of High Energy Resolution Fluorescence Detected XAS (HERFD-XAS) and Valence-to-Core X-ray Emission Spectroscopy (V2C XES) at the Cu K-edge under NH<sub>3</sub>-SCR operating conditions to shed light on the standard SCR mechanism over Cu-SSZ-13. For this purpose, we prepared a well-defined Cu-SSZ-13 catalyst and studied the structure at relevant SCR conditions and systematically under 12 defined reference conditions to understand the influence of each species and their interactions. The spectra were further interpreted using reference compounds and density-functional theory (DFT) calculations. In addition, we compare the results to our recent HERFD-XAS/XES study of Fe-ZSM-5.<sup>14b</sup>

The 1.2 wt% Cu-SSZ-13 catalyst was prepared by ion-exchange with copper acetate (ESI<sup>†</sup>) resulting in a Si:Al-ratio of 16:1 and Cu:Al = 0.2:1. EXAFS data analysis shows mostly isolated 4-fold coordinated Cu<sup>2+</sup> sites with a Cu–O bond distance around 1.96 Å (ESI<sup>†</sup> Fig. S3). This is in line with literature, where isolated sites were observed for the used ion exchange level, possibly close to 8 membered rings under the applied reaction conditions.<sup>16</sup> This catalyst sample demonstrated typical SCR activity with a seagull shaped light-off curve (ESI<sup>†</sup> Fig. S2). Next, the catalyst was tested in an operando fixed-bed quartz capillary microreactor cell.<sup>17</sup> These experiments were performed with a sieve fraction of 100–200 μm

<sup>a</sup> Institute for Chemical Technology and Polymer Chemistry (ITCP), Karlsruhe Institute of Technology, D-76131 Karlsruhe, Germany. E-mail: grunwaldt@kit.edu

<sup>b</sup> Institute of Catalysis Research and Technology (IKFT), Karlsruhe Institute of Technology, D-76344 Eggenstein-Leopoldshafen, Germany

<sup>c</sup> European Synchrotron Radiation Facility, F-38043 Grenoble Cedex, France

<sup>d</sup> Center for Functional Nanostructures and Institute of Physical Chemistry, Karlsruhe Institute of Technology, D-76131 Karlsruhe, Germany

<sup>e</sup> Institute of Physical and Theoretical Chemistry, TU Braunschweig, D-38106 Braunschweig, Germany

† Electronic supplementary information (ESI) available: Experimental details, synthesis, catalytic performance, EXAFS, DFT calculations. See DOI: 10.1039/c5cc01758k



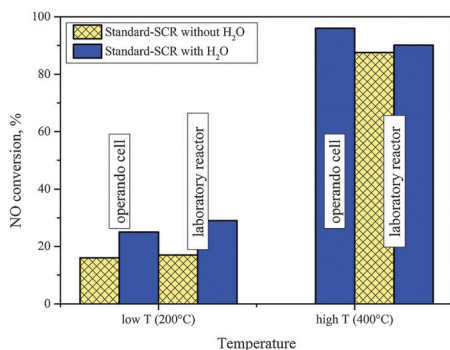


Fig. 1 Catalytic activity of 1.2 wt% Cu-SSZ-13 measured in the lab fixed-bed reactor and the operando cell at the beamline using 1000 ppm NO, 1000 ppm NH<sub>3</sub>, 10% O<sub>2</sub> and 0–1.5% H<sub>2</sub>O (GHSV 200 000 h<sup>-1</sup>, further details in the ESI†).

(ESI†) to avoid mass transfer limitations,<sup>17</sup> which can strongly influence SCR activity over Cu-zeolites.<sup>18</sup> The suitability of the approach is underlined by the results in Fig. 1 as the conversion of NO in the operando cell was close to that in the laboratory fixed-bed reactor and water enhanced the performance as known for Cu-SCR catalysts.<sup>13,19</sup>

The results obtained with XAS/XES are first described separately and afterwards correlated to obtain a coherent picture. The numbering of the conditions was chosen to present spectral differences and is not according to the experimental order. Before each experiment, the sample was treated to reach its initial state.

HERFD-XANES spectra were collected during NO and NH<sub>3</sub> oxidation, and under standard SCR with or without water (Fig. 2). At first glance, major changes of the XANES profiles are visible for conditions involving NH<sub>3</sub>. However, important variations could be observed for all investigated conditions. The HERFD-XANES spectrum of the untreated sample in synthetic air at room temperature (condition 1)

contains features typical for Cu-SSZ-13:<sup>8</sup> a pre-edge feature A at 8977.4 eV (1s → 3d transition in Cu<sup>2+</sup>),<sup>20</sup> a small shoulder B at 8982.7 eV (1s → 4p transition of two-coordinated Cu<sup>+</sup> sites)<sup>6a</sup> and a second shoulder C at 8986.5 eV (Cu<sup>2+</sup> 1s → 4p transition with ligand to metal charge transfer (LMCT, shakedown)).<sup>8,21</sup> A similar profile was recorded at 200 °C in the presence of water (cond. 4) which corresponds to hydrated Cu<sup>2+</sup> sites. Dehydration by pretreatment at 550 °C (cond. 2) led to a slightly higher intensity of the pre-edge and of the features B and C. The white-line showed a sharper main feature E around 8997 eV accompanied by a shoulder D at 8993 eV, indicating a slight difference in the coordination sphere.<sup>22</sup> Analysis of the pre-edge region indicates a majority of Cu<sup>2+</sup> sites present under these conditions. The removal of O<sub>2</sub> and H<sub>2</sub>O (cond. 3) led to a decrease of the pre-edge feature A suggesting autoreduction (about 60% Cu<sup>+</sup> as estimated by its integration, Fig. 2, Table).

With respect to the reactant gases, NO addition mainly affected features B and C. Thus dosing only NO + He (cond. 7) yielded the highest intensity of C but a diminishment of feature B in comparison to cond. 2 (O<sub>2</sub>/He). Both features B and C decrease when NO and O<sub>2</sub> are dosed over the catalyst bed, indicating the complete absence of Cu<sup>+</sup> species. This could be caused by oxidation of the remaining Cu<sup>+</sup> sites by traces of NO<sub>2</sub>. Moreover, shoulder C almost vanishes upon addition of H<sub>2</sub>O. These results preclude the reduction of the Cu sites by NO at 200 °C. As reduction of the Cu<sup>2+</sup> sites is expected during the SCR-reaction, the adsorption of NO on Cu<sup>+</sup> species was verified after reduction at 550 °C in 5% H<sub>2</sub>/He (cond. 13). Note that the corresponding HERFD-XANES shows a shoulder around 8981 eV probably due to overreduction to Cu<sup>0</sup>.<sup>22,23</sup>

The second group of spectra, which involve NH<sub>3</sub> (cond. 8–12), exhibit an intense feature B suggested to originate from linear coordination to the Cu sites.<sup>8,21,24</sup> The highest intensity of feature B was observed in NH<sub>3</sub>-He (cond. 9) combined with an almost

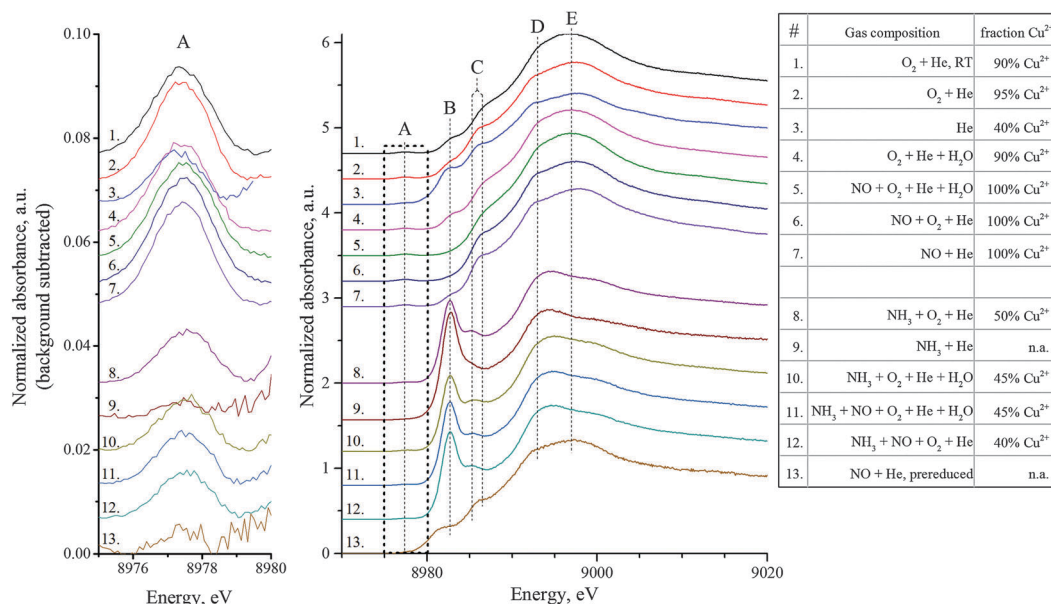


Fig. 2 Cu K-edge HERFD-XANES (middle) and pre-edge region (left) of Cu-SSZ-13 during NH<sub>3</sub>-SCR and under model gas mixtures at 200 °C (exact gas composition and temperature given in the ESI,† Table S2). Estimation of Cu<sup>2+</sup> amount (±10%) relative to all Cu in the sample based on the integral of the background-subtracted pre-edge peak (at 8977.4 eV) taking the spectra of conditions 1, 2, 4–7 as Cu<sup>2+</sup> reference (details, cf. ESI†).



complete disappearance of the pre-edge feature A, which strongly suggests reduction of  $\text{Cu}^{2+}$  species. The addition of  $\text{NH}_3$  (cond. 8, 10) to the oxidizing atmosphere also led to reduced intensity in the  $1s \rightarrow 3d$  pre-edge region, combined with a shift of this feature by 0.2 eV to higher energies, which is possibly due to structural distortion or higher ligand field splitting.<sup>25</sup> The presence of  $\text{H}_2\text{O}$  and  $\text{O}_2$  in the gas mixture led to a stepwise decrease of feature B (higher coordination, more oxidized). As no  $\text{NH}_3$  oxidation is observed at this temperature, a reaction can be excluded, suggesting a competitive (or three-fold) adsorption of  $\text{NH}_3$  and  $\text{H}_2\text{O}$  at the Cu-sites as also observed by  $\text{NH}_3$ -TPD (ESI,† Fig. S16) and shown for other Cu-systems.<sup>26</sup>

Dosing the standard SCR gas mixture  $\text{NO} + \text{NH}_3 + \text{O}_2$  (cond. 12, 18%  $\text{NO}_x$  conversion) resulted in a spectrum similar to  $\text{NH}_3 + \text{O}_2$  (cond. 8), only a little decrease of the main feature B was observed. The more realistic gas mixture with water (cond. 11) led to a spectrum similar to  $\text{NH}_3 + \text{O}_2 + \text{H}_2\text{O}$  (cond. 10).

Next, we focused on the X-ray emission spectra (Fig. 3). Similarly to the HERFD-XANES results, the spectra can be divided into two groups showing similar features, *i.e.* catalyst without  $\text{NH}_3$  in the feed (cond. 1–7, 13) and catalyst with  $\text{NH}_3$  in the feed (cond. 8–12, including SCR). The differences between those groups are the following: (a) appearance of a second peak upon  $\text{NH}_3$  addition in the  $\text{K}\beta''$  region at 8958.3 eV which is seen either as broadening of peak 8956.9 eV (both peaks have similar intensity in cond. 9–11) or a shift of this peak (dominating over the peak at 8956.9 eV in cond. 8 and 12). These features are similar to those reported during *in situ* adsorption of  $\text{NH}_3$  on Cu-SSZ-13 by Giordanino *et al.*<sup>8</sup> and can be attributed to an N atom in the coordination sphere of Cu, *i.e.* direct adsorption of  $\text{NH}_3$ . DFT-calculations on the influence of the ligand environment on the XES spectra support such an assignment (ESI,† Fig. S10). No feature stemming from ammonia adsorbed *via* hydroxyl groups was detected for copper. This is in contrast to the

$\text{Fe-O}^+\text{H-NH}_x$  moiety observed for Fe-ZSM-5.<sup>14b</sup> (b) A peak at 8972.3 eV in the  $\text{K}\beta_{2,5}$  region which is shifted to 8973.4 eV and becomes more intense upon removal of reactants with only  $\text{NH}_3/\text{He}$  remaining, (c) increased intensity of features at 8981.6 and 8990.0 eV after adsorption of  $\text{NH}_3$ , probably due to a change in geometry of the Cu complex. The changes named above stem only from interaction with ammonia but not from the change of Cu oxidation state which is verified by exp. 13 (*vs.* exp. 7) where no significant changes are observed after NO-adsorption on pre-reduced Cu.

Mainly minor changes in relative intensity of the  $\text{K}\beta_{2,5}$  peaks were observed for the group of spectra recorded in  $\text{NH}_3$ -free atmosphere. The addition of NO (in He) caused broadening or diminishment of the  $\text{K}\beta''$  features compared to the dehydrated catalyst in He. However, no clear peak at 8958.3 eV from an N atom was noted upon adsorption of NO (cond. 7). In the presence of  $\text{O}_2$  and  $\text{H}_2\text{O}$ , the peak at 8956.9 eV showed basically no change upon NO addition. This indicates a strong inhibition effect particularly due to  $\text{H}_2\text{O}$  (ESI,† Fig. S12, ref. 13) and points to weak adsorption of NO probably *via* the O atom as isonitrosyl, accompanied by small changes in the coordination environment of Cu sites.

Strikingly different from the case of NO and  $\text{NH}_3$  adsorption over Fe-ZSM-5 is the absence of a  $\text{K}\beta''$  peak at low energy which we ascribed to a positively polarized/triple coordinated oxygen atom with NO bound *via* Fe-O.<sup>14b</sup> This difference in adsorption of NO on Fe- and Cu-zeolites is substantial and may explain the debated differences in SCR performance and also in NO oxidation activity of those zeolites.<sup>27</sup> Indeed, NO adsorbs *via* an additional O atom as a nitrite-like intermediate on an Fe site and then can be readily desorbed as  $\text{NO}_2$ , whereas in the case of Cu NO seems to be adsorbed as a nitroso-group and, hence, can desorb easily again as NO or react with adsorbed  $\text{NH}_3$ . DRIFTS has recently evidenced  $\text{NO}^+$  on Cu-CHA catalysts.<sup>4c,13</sup>

In summary, we observed strong  $\text{NH}_3$  adsorption on Cu sites under all conditions involving ammonia, the intensity of the  $\text{NH}_3$ -related XANES features was lower for the feeds containing water. The positive influence of  $\text{H}_2\text{O}$  evidenced also earlier<sup>5,19,29</sup> can be caused either by inhibition of  $\text{NH}_3$  adsorption or by an increased  $\text{Cu}^+$  reoxidation rate.<sup>28</sup> Concerning NO, its adsorption is supported by the change of shape of the  $\text{K}\beta''$  peak and also of the HERFD-XANES spectra (cond. 7 *vs.* 3). However, in the presence of  $\text{O}_2$  and/or  $\text{H}_2\text{O}$  (cond. 5 and 6) only the relative intensities of peaks in the  $\text{K}\beta_{2,5}$  region changed and the NO adsorption must be weak. Those small changes are completely indiscernible behind the features arising from  $\text{NH}_3$  and therefore in the current state of work we assume that either NO is weakly adsorbed, or rapidly reacts from the gas phase with adsorbed ammonia/amino groups.

The proposed mechanism depicted in Scheme 1 only partially supports the mechanism suggested by Gao *et al.*<sup>3</sup> since the formation of  $\text{NH}_3\text{-Cu}^+\text{-NO}^+$  could not be unambiguously demonstrated. Thus, the presented data indicate that during standard SCR,  $\text{NH}_3$  adsorbs on a  $\text{Cu}^{2+}$  site *via* direct coordination. Next, NO may adsorb on the same site *via* O and react with  $\text{NH}_3$  or directly react from the gas phase as suggested by several previous studies.<sup>6a,9,30</sup> Both paths could circumvent the blockage of the Cu sites at low temperatures by  $\text{NH}_3$ , which is in contrast to the Fe-ZSM-5 case, where the strong  $\text{NH}_3$ -adsorption (ESI,† Fig. S15) additionally

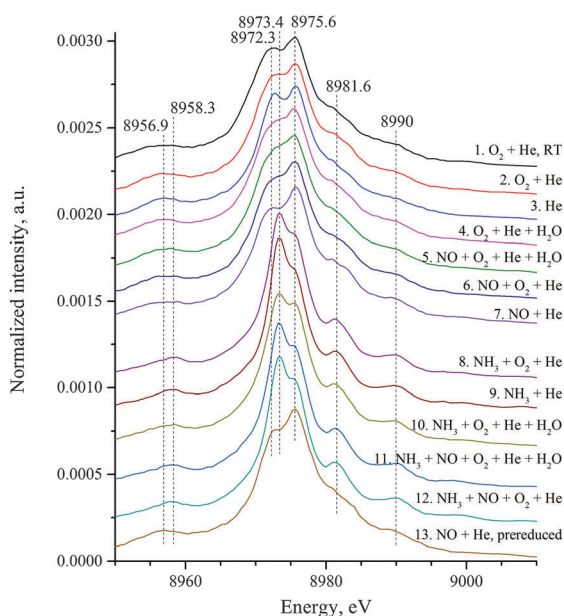
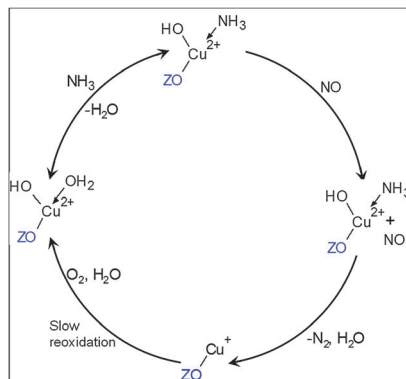


Fig. 3 XES spectra of Cu-SSZ-13 catalyst during  $\text{NH}_3$ -SCR and under related model gas mixtures at 200 °C (exact composition and temperature given in the ESI,† Table S2).





**Scheme 1** Role of copper in Cu-SSZ-13 suggested by operando XES and XAS during  $\text{NH}_3$ -SCR. Possible additional water–ammonia ligands are left out for clarity. ZO stands for zeolite cation-exchange site.

inhibits the reoxidation. NO might be activated by direct interaction with  $\text{NH}_3$  or weakly adsorbed *via* Cu-O. The decomposition of the formed nitrosoamide<sup>3</sup> intermediate may be facilitated by the presence of water (Fig. 1) *via* an ammonium nitrite formation and subsequent thermal decomposition (not shown) or because it promotes the mobility and stabilizes the resulting undercoordinated  $\text{Cu}^+$ . As a result of SCR and its electron transfer processes, a reduced  $\text{Cu}^+$  site with low coordination number is found, in accordance with the spatially-resolved XAS study of Cu-SAPO-34,<sup>7</sup> which is then oxidized by  $\text{O}_2$  (no proof of  $\text{NO}_x$  participation was found) to  $\text{Cu}^{2+}$  as a slow and rate-limiting step and stabilized by  $\text{H}_2\text{O}$  as  $\text{Cu}^{2+}\text{-OH}$ .<sup>4c</sup> In contrast, for Fe-ZSM-5 coordination of NO and  $\text{NH}_3$  *via* Cu-O has been suggested which could not be found for Cu in Cu-SSZ-13.

By combining operando HERFD-XAS and V2C XES we could provide important new insight into the structure of copper and its interaction with  $\text{NH}_3$  and NO during standard SCR. A significant difference in the intermediate species during SCR over Fe-ZSM-5 and Cu-SSZ-13 was found. This difference could explain the higher activity of Cu-zeolites at low temperatures and the absence of an  $\text{NH}_3$  inhibition effect. Furthermore, it could be correlated with the different NO oxidation behavior of the Fe- and Cu-zeolites. In future, it would be valuable to extend these studies to V-SCR catalysts and exploit the same approach of combining operando HERFD-XANES, XES and DFT calculations.

This work has been supported by KIT, the Federal Ministry of Education and Research (BMBF, projects 05K10VKB and 05K13VK2) and DBU (T. Günter). We thank ESRF for providing the beamtime at the ID26 beamline and financial support at ESRF and C. Lapras for the technical support. We are also grateful to E. Japke for the assistance during XES measurements and T. Bergfeldt (IAM-AWP, KIT) for elemental analysis.

## Notes and references

- 1 (a) I. Nova and E. Tronconi, *Urea-SCR Technology for deNO<sub>x</sub> After Treatment of Diesel Exhausts*, Springer, New York, 2014; (b) U. Deka, I. Lezcano-Gonzalez, B. M. Weckhuysen and A. M. Beale, *ACS Catal.*, 2013, **3**, 413.

- 2 (a) P. G. Blakeman, E. M. Burkholder, H.-Y. Chen, J. E. Collier, J. M. Fedeyko, H. Jobson and R. R. Rajaram, *Catal. Today*, 2014, **231**, 56; (b) S. J. Schmieg, S. H. Oh, C. H. Kim, D. B. Brown, J. H. Lee, C. H. F. Peden and D. H. Kim, *Catal. Today*, 2012, **184**, 252.
- 3 F. Gao, J. Kwak, J. Szanyi and C. H. F. Peden, *Top. Catal.*, 2013, **56**, 1441.
- 4 (a) F. Gao, E. D. Walter, E. M. Karp, J. Luo, R. G. Tonkyn, J. H. Kwak, J. Szanyi and C. H. F. Peden, *J. Catal.*, 2013, **300**, 20; (b) S. A. Bates, A. A. Verma, C. Paolucci, A. A. Parekh, T. Anggara, A. Yezzerets, W. F. Schneider, J. T. Miller, W. N. Delgass and F. H. Ribeiro, *J. Catal.*, 2014, **312**, 87; (c) R. Zhang, J.-S. McEwen, M. Kollár, F. Gao, Y. Wang, J. Szanyi and C. H. F. Peden, *ACS Catal.*, 2014, **4**, 4093.
- 5 F. Gao, E. D. Walter, M. Kollar, Y. Wang, J. Szanyi and C. H. F. Peden, *J. Catal.*, 2014, **319**, 1.
- 6 (a) C. Paolucci, A. A. Verma, S. A. Bates, V. F. Kispersky, J. T. Miller, R. Gounder, W. N. Delgass, F. H. Ribeiro and W. F. Schneider, *Angew. Chem., Int. Ed.*, 2014, **53**, 11828; (b) J. S. McEwen, T. Anggara, W. F. Schneider, V. F. Kispersky, J. T. Miller, W. N. Delgass and F. H. Ribeiro, *Catal. Today*, 2012, **184**, 129.
- 7 D. E. Doronkin, M. Casapu, T. Günter, O. Müller, R. Frahm and J.-D. Grunwaldt, *J. Phys. Chem. C*, 2014, **118**, 10204.
- 8 F. Giordanino, E. Borfecchia, K. A. Lomachenko, A. Lazzarini, G. Agostini, E. Gallo, A. V. Soldatov, P. Beato, S. Bordiga and C. Lamberti, *J. Phys. Chem. Lett.*, 2014, **5**, 1552.
- 9 H. Sjövall, E. Fridell, R. Blint and L. Olsson, *Top. Catal.*, 2007, **42–43**, 113.
- 10 (a) L. Shi, T. Yu, X. Wang, J. Wang and M. Shen, *Acta Phys.-Chim. Sin.*, 2013, **29**, 1550; (b) H. Zhu, J. H. Kwak, C. H. F. Peden and J. Szanyi, *Catal. Today*, 2013, **205**, 16.
- 11 J. Szanyi, J. H. Kwak, H. Zhu and C. H. F. Peden, *Phys. Chem. Chem. Phys.*, 2013, **15**, 2368.
- 12 T. Yu, T. Hao, D. Fan, J. Wang, M. Shen and W. Li, *J. Phys. Chem. C*, 2014, **118**, 6565.
- 13 M. P. Ruggeri, I. Nova, E. Tronconi, J. A. Pihl, T. J. Toops and W. P. Partridge, *Appl. Catal., B*, 2015, **166–167**, 181.
- 14 (a) V. F. Kispersky, A. J. Kropf, F. H. Ribeiro and J. T. Miller, *Phys. Chem. Chem. Phys.*, 2012, **14**, 2229; (b) A. Boubnov, H. W. P. Carvalho, D. E. Doronkin, T. Günter, E. Gallo, A. J. Atkins, C. R. Jacob and J.-D. Grunwaldt, *J. Am. Chem. Soc.*, 2014, **136**, 13006.
- 15 (a) P. Glatzel and U. Bergmann, *Coord. Chem. Rev.*, 2005, **249**, 65; (b) N. Lee, T. Petrenko, U. Bergmann, F. Neese and S. DeBeer, *J. Am. Chem. Soc.*, 2010, **132**, 9715; (c) M. Bauer, *Phys. Chem. Chem. Phys.*, 2014, **16**, 13827.
- 16 E. Borfecchia, K. A. Lomachenko, F. Giordanino, H. Falsig, P. Beato, A. V. Soldatov, S. Bordiga and C. Lamberti, *Chem. Sci.*, 2015, **6**, 548.
- 17 J. D. Grunwaldt, M. Caravati, S. Hannemann and A. Baiker, *Phys. Chem. Chem. Phys.*, 2004, **6**, 3037.
- 18 P. S. Metkar, V. Balakotaiah and M. P. Harold, *Chem. Eng. Sci.*, 2011, **66**, 5192.
- 19 H. Sjövall, L. Olsson, E. Fridell and R. J. Blint, *Appl. Catal., B*, 2006, **64**, 180.
- 20 E. M. C. Alayon, M. Nachttegaal, E. Kleymenov and J. A. van Bokhoven, *Microporous Mesoporous Mater.*, 2013, **166**, 131.
- 21 L. S. Kau, D. J. Spira-Solomon, J. E. Penner-Hahn, K. O. Hodgson and E. I. Solomon, *J. Am. Chem. Soc.*, 1987, **109**, 6433.
- 22 N. B. Castagnola, A. J. Kropf and C. L. Marshall, *Appl. Catal., A*, 2005, **290**, 110.
- 23 M. K. Neylon, C. L. Marshall and A. J. Kropf, *J. Am. Chem. Soc.*, 2002, **124**, 5457.
- 24 R. A. Himes, G. Y. Park, A. N. Barry, N. J. Blackburn and K. D. Karlin, *J. Am. Chem. Soc.*, 2007, **129**, 5352.
- 25 K.-I. Shimizu, H. Maeshima, H. Yoshida, A. Satsuma and T. Hattori, *Phys. Chem. Chem. Phys.*, 2001, **3**, 862.
- 26 (a) P. Kappen, J.-D. Grunwaldt, B. S. Hammershøi, L. Tröger and B. S. Clausen, *J. Catal.*, 2001, **198**, 56; (b) R. Kumashiro, Y. Kuroda and M. Nagao, *J. Phys. Chem. B*, 1998, **103**, 89.
- 27 M. Ruggeri, I. Nova and E. Tronconi, *Top. Catal.*, 2013, **56**, 109.
- 28 G. T. Palomino, P. Fiscaro, S. Bordiga, A. Zecchina, E. Giamello and C. Lamberti, *J. Phys. Chem. B*, 2000, **104**, 4064.
- 29 (a) J. A. Sullivan, J. Cunningham, M. A. Morris and K. Keneavey, *Appl. Catal., B*, 1995, **7**, 137; (b) A. V. Salker and W. Weisweiler, *Appl. Catal., A*, 2000, **203**, 221.
- 30 L. Xu, R. W. McCabe and R. H. Hammerle, *Appl. Catal., B*, 2002, **39**, 51.

